SC-RR-67-2961

C10 #5413

OSTI 4530272

AEROSPACE NUCLEAR SAFETY

SC-RR-67-2961

February 1968

AN ANALYSIS OF THE INCREASED AERODYNAMIC HEATING TO THE SNAP-27 GRAPHITE LUNAR MODULE FUEL CASK (GLFC) RESULTING FROM THE TITANIUM MOUNTING STRUCTURE

Aerospace Nuclear Safety
Information Center
Accession No.
01728-01
Sandia Corporation

H. R. Spahr, 9314

DO NOT DESTROY
Return to
Aerospace Nuclear Safety
Information Center

SANDIA LABORATORIES

OPERATED FOR THE UNITED STATES ATOMIC ENERGY COMMISSION BY SANDIA CORPORATION | ALBUQUERQUE, NEW MEXICO, LIVERMORE, CALIFORNIA

Issued by Sandia Corporation,
a prime contractor to the
United States Atomic Energy Commission

LEGAL NOTICE

This report was prepared as an account of Government sponsored work. Neither the United States, nor the Commission, nor any person acting on behalf of the Commission:

A. Makes any warranty or representation, expressed or implied, with respect to the accuracy, completeness, or usefulness of the information contained in this report, or that the use of any information, apparatus, method, or process disclosed in this report may not infringe privately owned rights; or

B. Assumes any liabilities with respect to the use of, or for damages resulting from the use of any information, apparatus, method, or process disclosed in this report.

As used in the above, "person acting on behalf of the Commission" includes any employee or contractor of the Commission, or employee of such contractor, to the extent that such employee or contractor of the Commission, or employee of such contractor prepares, disseminates, or provides access to, any information pursuant to his employment or contract with the Commission, or his employment with such contractor.

Printed in the United States of America
Available from
Clearinghouse for Federal Scientific and Technical Information
Springfield, Virginia 22151
Price: Printed Copy $3.00; Microfiche $0.65

SC-RR-67-2961

AN ANALYSIS OF THE INCREASED AERODYNAMIC HEATING TO THE SNAP-27 GRAPHITE LUNAR MODULE FUEL CASK (GLFC) RESULTING FROM THE TITANIUM MOUNTING STRUCTURE

H. R. Spahr, 9314
Sandia Laboratory, Albuquerque

February, 1968

ABSTRACT

This report presents a theoretical analysis which defines the increased aerodynamic heating rates resulting from the SNAP-27 GLFC titanium mounting structure. Local and "average" aerodynamic heating rate distributions in front of a protuberance are presented for six flight conditions. The "average" aerodynamic heating rates immediately in front of a protuberance are approximately ten times the stagnation line aerodynamic heating rate to a GLFC reentering crosswise.

DIST 2 GAPRBS

j

SUMMARY

In the Aerospace Nuclear Safety Program, aerothermodynamic analyses are made to determine the behavior of nuclear systems during launch aborts and reentry after use in space. These analyses define the aerothermodynamic history of the reentering nuclear system and attached hardware.

Such an analysis, conducted for the SNAP-27 graphite lunar module fuel cask (GLFC), showed that the titanium mounting struts can remain with the GLFC during a significant portion of the reentry. This analysis assumed that the heating rates to the titanium bands and GLFC were the rates that would exist on a crosswise spinning GLFC without the support structure.

Since there is no active effort to modify the mounting hardware to insure that it separates from the GLFC at relatively high altitudes, a more refined aerothermodynamic analysis was made. This aerothermodynamic analysis required that an aerodynamic analysis be performed to define the "average" aerodynamic heating rates to the GLFC in front of a protuberance on the titanium mounting structure. These "average" aerodynamic heating rates were calculated for six flight conditions, and are up to approximately 10 times the stagnation line aerodynamic heating rate to a GLFC reentering crosswise.

TABLE OF CONTENTS

	Page
Introduction	5
Flight Conditions Investigated	9
The Configuration Analyzed	11
A Description of the Flow Field	12
Free Stream Conditions in Front of the GLFC Bow Shock Wave	12
Stagnation Conditions Behind the GLFC Bow Shock Wave	16
Local Free Stream Conditions in Front of the Protuberance Secondary Bow Shock Wave	17
Stagnation Conditions Behind the Protuberance Secondary Bow Shock Wave	21
Reference Conditions in the Reversed Flow Region	23
Calculation of the Aerodynamic Heating Rate Distribution in Front of the Protuberance	26
Calculation of the "Average" Aerodynamic Heating Rate in Front of the Protuberance	28
Calculation of the Ratio of "Average" Aerodynamic Heating in Front of the Protuberance to the Stagnation Line Aerodynamic Heating Rate to the GLFC	33
Conclusions	35
References	37

AN ANALYSIS OF THE INCREASED AERODYNAMIC HEATING TO THE SNAP-27 GRAPHITE LUNAR MODULE FUEL CASK (GLFC) RESULTING FROM THE TITANIUM MOUNTING STRUCTURE

Introduction

As part of the NASA APOLLO program, the APOLLO Lunar Surface Experiment Package (ALSEP) (Figure 1) will gather data regarding the characteristics and environment of the lunar surface and subsurface. References 1 and 2 describe, in some detail, the different experiments which are part of this package.

The ALSEP package gathers and transmits data for a one year period. The AEC is developing the SNAP-27 radioisotope thermoelectric generator to supply electrical power for the ALSEP package. General Electric Co. (GE) is designing and fabricating the SNAP-27 generator, fuel capsule, and graphite lunar module fuel cask (GLFC) under AEC contract.

The SNAP-27 fuel capsule (Figure 2) is contained in the GLFC (Figure 3) during transport to the lunar surface. Titanium struts and bands attach the GLFC to the lunar module.

As is done for all SNAP systems, the Reentry and Space Sciences Division of the Sandia Corporation Aerospace Nuclear Safety Department conducted a number of aerothermodynamic analyses of the SNAP-27 GLFC and attached hardware. One of these analyses showed that the titanium structure would remain with the GLFC throughout an appreciable portion of the reentry. This analysis assumed that the heating rates to the titanium bands and GLFC were the rates that would exist on a crosswise spinning GLFC without the titanium structure and that the titanium band temperature was the same as the GLFC surface temperature.

Since there is no active effort to modify the mounting hardware to insure that it separates from the GLFC at relatively high altitudes, a more refined aerothermodynamic analysis was made. This aerothermodynamic analysis required the definition of "average" aerodynamic heating rates to the GLFC in front of a protuberance on the titanium mounting structure.

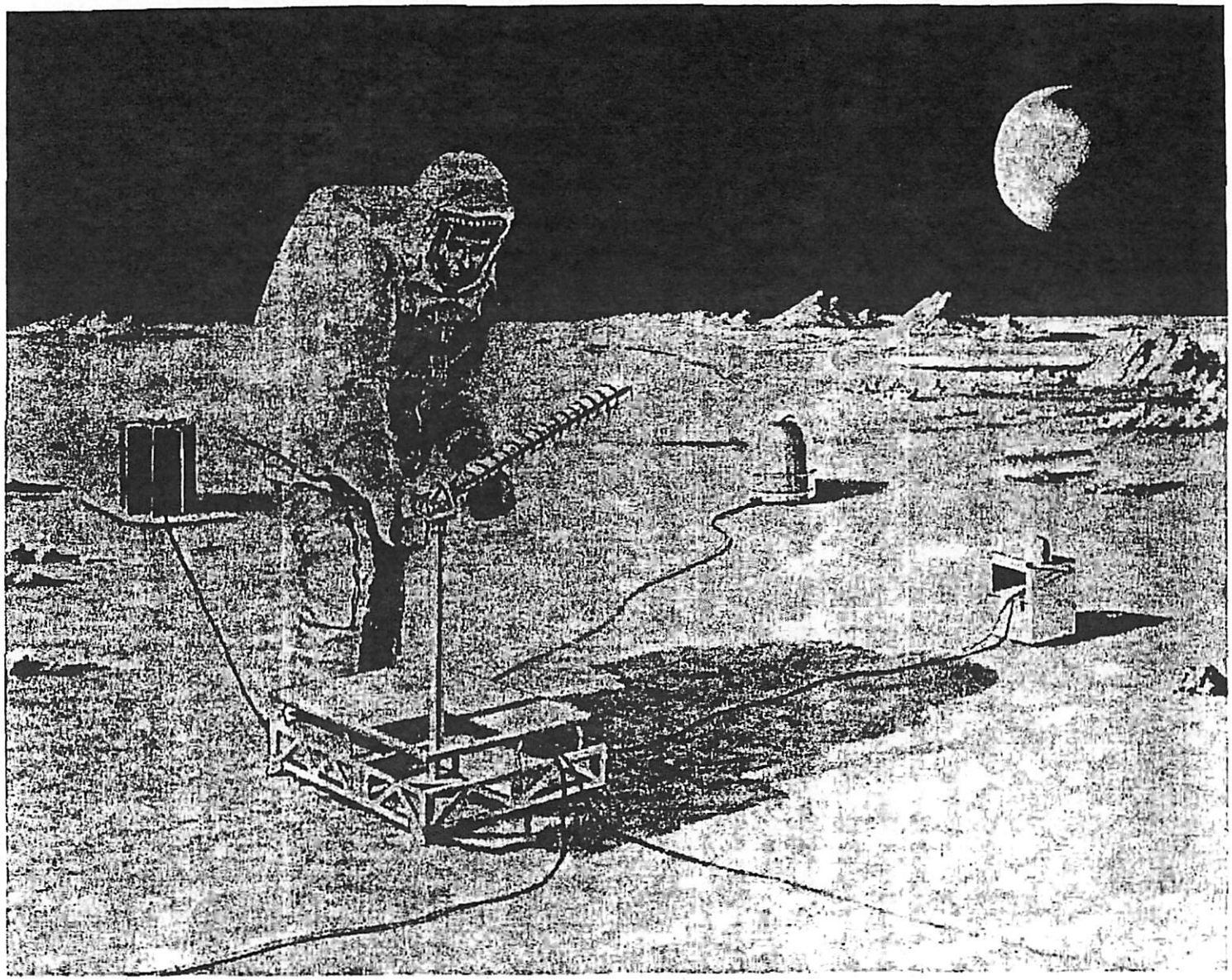

Figure 1. APOLLO Lunar Surface Experiment Package Array
(C66-4608)

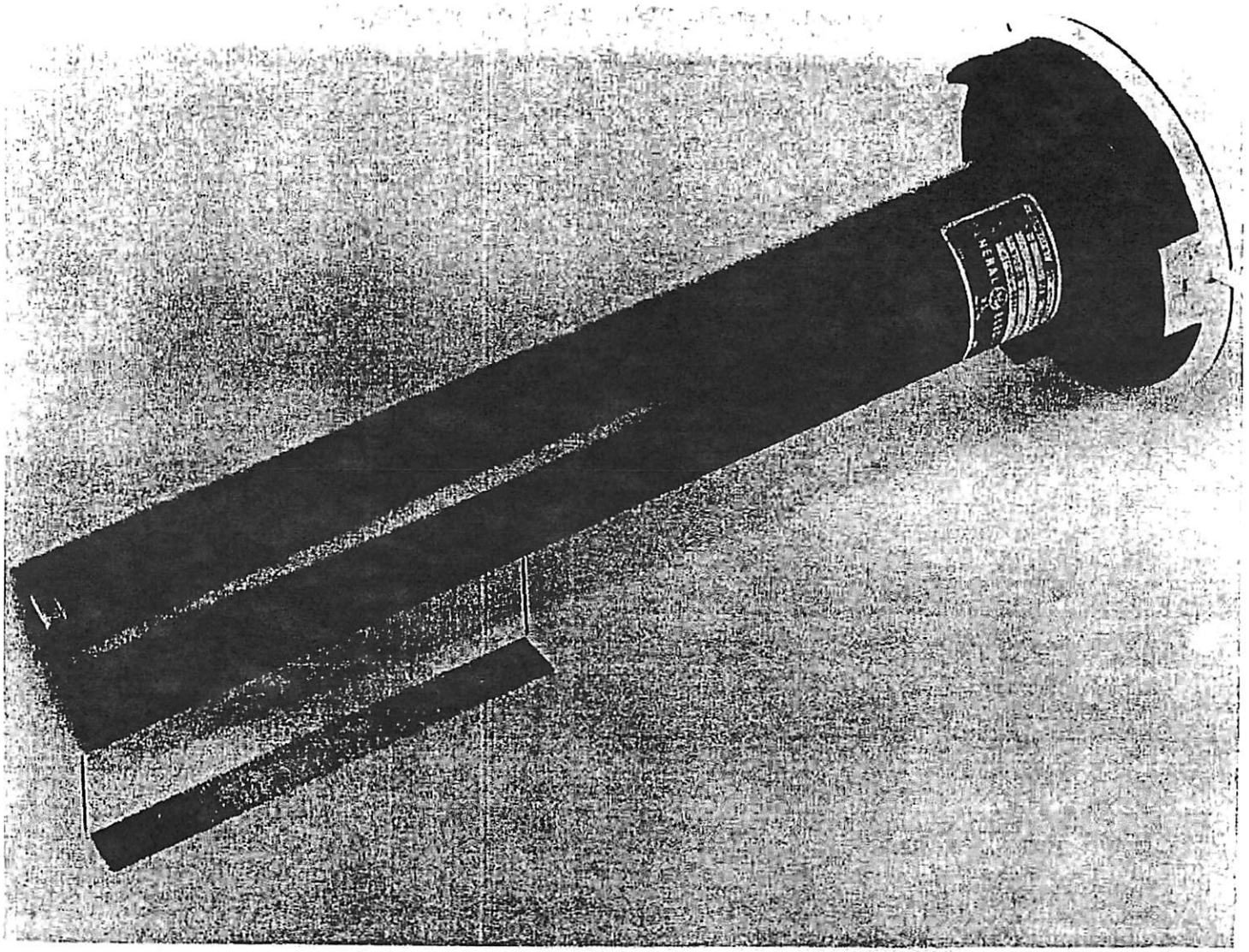

Figure 2. SNAP-27 Fuel Capsule
(D66-2638)

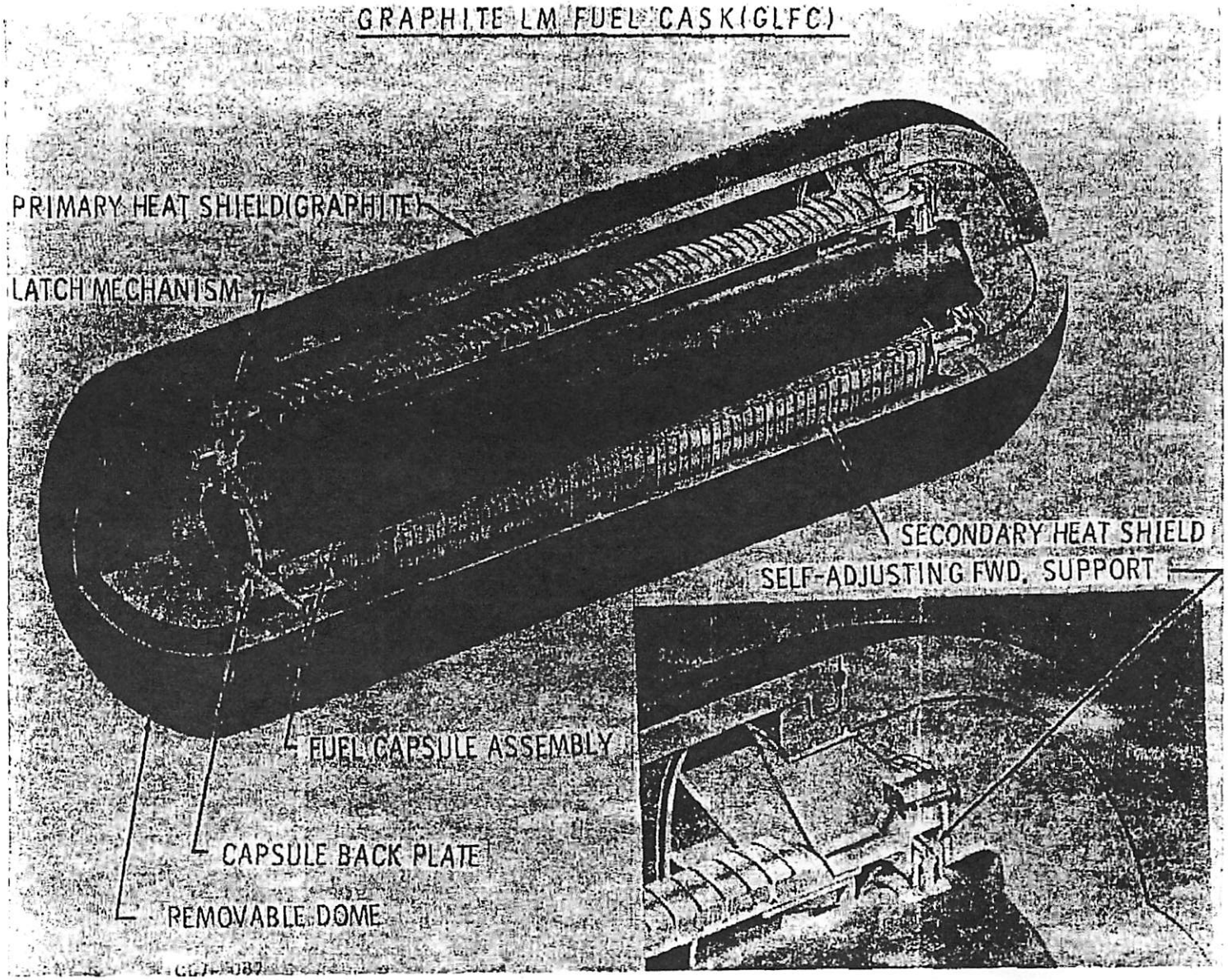

Figure 3. SNAP-27 Graphite Lunar Module Fuel Cask (GLFC) (C67-8087)

Since the Reentry and Space Sciences Division had been asked to make a presentation at a meeting to discuss potential problem areas on the SNAP-27 GLFC at NASA/MSC in Houston on November 7, 1967, the complete aerothermodynamic analysis had to be completed by November 6, 1967. The time required for the remaining parts of this complete analysis limited the time available for the definition of the increased heating rates to approximately two days.

The following sections of this report document the theoretical aerodynamic analysis which defined the "average" aerodynamic heating rates to the GLFC in front of a protuberance on the titanium mounting structure.

Flight Conditions Investigated

In aerothermodynamic analyses of the GLFC, three reentries are typically investigated. The orbital decay reentry trajectory uses lunar module drag data (Reference 3) for the crosswise reentry mode of the lunar module descent stage (with 80 percent full fuel tanks) down to an altitude of 300,000 feet where the descent stage is assumed to disassemble. Previous work showed that 300,000 feet is the lowest altitude at which lunar module disassembly is expected. The drag data for the GLFC in crossflow are then used down to impact. Initial conditions for the orbital decay at 400,000 feet altitude are obtained using the HRS004 (References 4 and 5) computer code. Sandia's latest GLFC orbital decay trajectory, number 17703, was used.

The second trajectory typically investigated is the smallest possible reentry angle supercircular velocity reentry. This is a -6.25 degree inertial geodetic reentry angle at 400,000 feet altitude at an inertial velocity of 36,333 feet per second. The lunar module configuration for this reentry is the ascent and descent stages together, crosswise, with full fuel tanks on both stages. Based on previous work, this lunar module configuration is assumed to disassemble at 330,000 feet. GLFC characteristics are then used to impact. Sandia's latest GLFC smallest possible reentry angle supercircular velocity reentry trajectory, number 17704, was used.

The third trajectory typically investigated is the largest "probable" reentry angle supercircular velocity reentry. This is a -38.05 degree inertial geodetic reentry angle at 400,000 feet altitude at an inertial velocity of 36,333 feet per second. The lunar module

configuration for this reentry is the ascent and descent stages together, crosswise, with full fuel tanks on both stages. Based on previous work, this lunar module configuration is assumed to disassemble at 330,000 feet. GLFC characteristics are then used to impact. Sandia's latest GLFC largest "probable" reentry angle supercircular velocity reentry trajectory, number 17705, was used.

Ideally, one would like to calculate the increased aerodynamic heating rate in front of the protuberance for a large number of points for each of the three trajectories. Time limitations made this impossible. Therefore, the flight conditions near maximum convective aerodynamic heating and near maximum deceleration were selected as points of special interest for each of the three trajectories. (Maximum convective aerodynamic heating is selected because maximum radiative aerodynamic heating is less than about 10 percent of the total aerodynamic heating for all three trajectories.) These flight conditions are in or near the continuum flow regime where the increased heating rate due to the protuberance is most important. These six flight conditions are:

A. Orbital decay, maximum convective aerodynamic heating
   V_∞ = air relative velocity
   = 20,000 feet per second
   h = altitude above mean sea level
   = 210,000 feet

B. Orbital decay, maximum deceleration
   V_∞ = 10,000 feet per second
   h = 150,000 feet

C. Shallow supercircular reentry, maximum convective aerodynamic heating
   V_∞ = 31,000 feet per second
   h = 200,000 feet

D. Shallow supercircular reentry, maximum deceleration
   V_∞ = 23,000 feet per second
   h = 170,000 feet

E. Steep supercircular reentry, maximum convective aerodynamic heating
   V_∞ = 31,000 feet per second
   h = 140,000 feet

F. Steep supercircular reentry, maximum deceleration
V_∞ = 20,000 feet per second
h = 100,000 feet

The Configuration Analyzed

The GLFC with the titanium mounting structure is shown in Bendix drawing BSX-5595 (Reference 6). This drawing shows a number of protuberances of various shapes and sizes. The protuberances selected for the analysis are the four "protuberances" at the intersections of the radial and longitudinal bands. These protuberances are approximated by a 1-1/2 inch diameter cylinder 1-1/4 inch long whose axis is normal to the cask surface.

The titanium struts, bands, and other hardware tend to stabilize the cask in roll, pitch, and yaw. Thus, it is assumed that the cask and hardware reenter with the cask axis of symmetry normal to the free stream velocity vector. The free stream velocity vector is assumed to be in the plane of symmetry of the cradle, with the struts and cradle on the "back side" of the cask. For these assumptions, the leading edge of the protuberance cylinder is approximately 73.5 degrees from the cask stagnation line. Figure 4 shows an end view of the configuration analyzed.

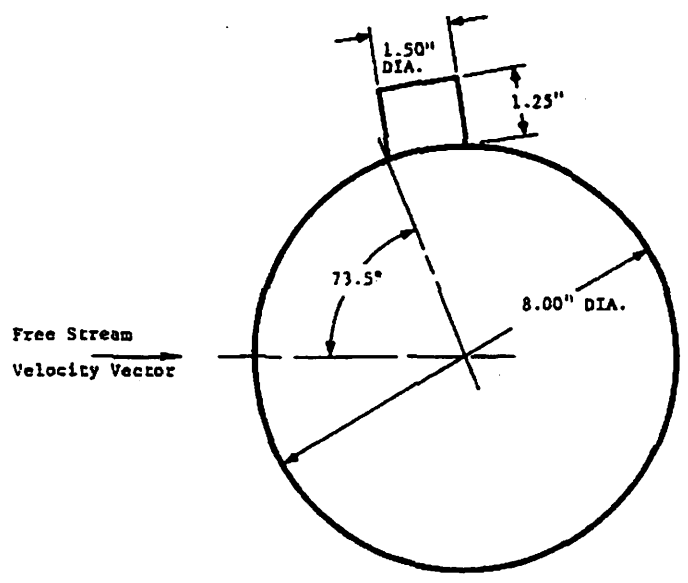

Figure 4. End View of GLFC and Protuberance Configuration Analyzed (D68-11285)

A Description of the Flow Field

Figure 5 shows the flow field around the GLFC with protuberance. Both the GLFC bow shock wave and the secondary bow shock wave in front of the protuberance are shown, as is the boundary layer on the GLFC.

Location (1) in Figure 5 is in the free stream ahead of the GLFC; at location (1), the free stream static flow field conditions will be of interest. Location (2) is at the stagnation line of the GLFC (i.e., behind the bow shock wave); at location (2), the local stagnation flow field conditions will be of interest. Location (3) is just ahead of the secondary bow shock wave in front of the protuberance and just outside the boundary layer; at location (3), the local static flow field conditions will be of interest. Location (4) is on the stagnation line of the protuberance cylinder and just outside the GLFC boundary layer; at location (4), the local stagnation flow field conditions will be of interest. Location (5) is on the stagnation line of the protuberance cylinder, but is inside the boundary layer of the GLFC; at location (5), the local stagnation flow field conditions will be of interest. Location (5) is where one should evaluate the "average" or reference boundary layer properties, as will be discussed later.

Figure 6 shows the flow field just in front of the protuberance cylinder. This region of reversed flow directly in front of the protuberance cylinder is the area for which the "average" increased aerodynamic heating will be calculated.

The following sections present the flow conditions at the five locations defined above. The techniques used to calculate these flow conditions are also presented.

Free Stream Conditions in Front of the GLFC Bow Shock Wave

To define the free stream conditions in front of the GLFC bow shock wave, one must refer to a set of atmospheric data tables. For this analysis, the 1962 U.S. Standard Atmosphere (Reference 7) was used to define the free stream air properties. These free stream air properties are presented below for the six flight conditions investigated.

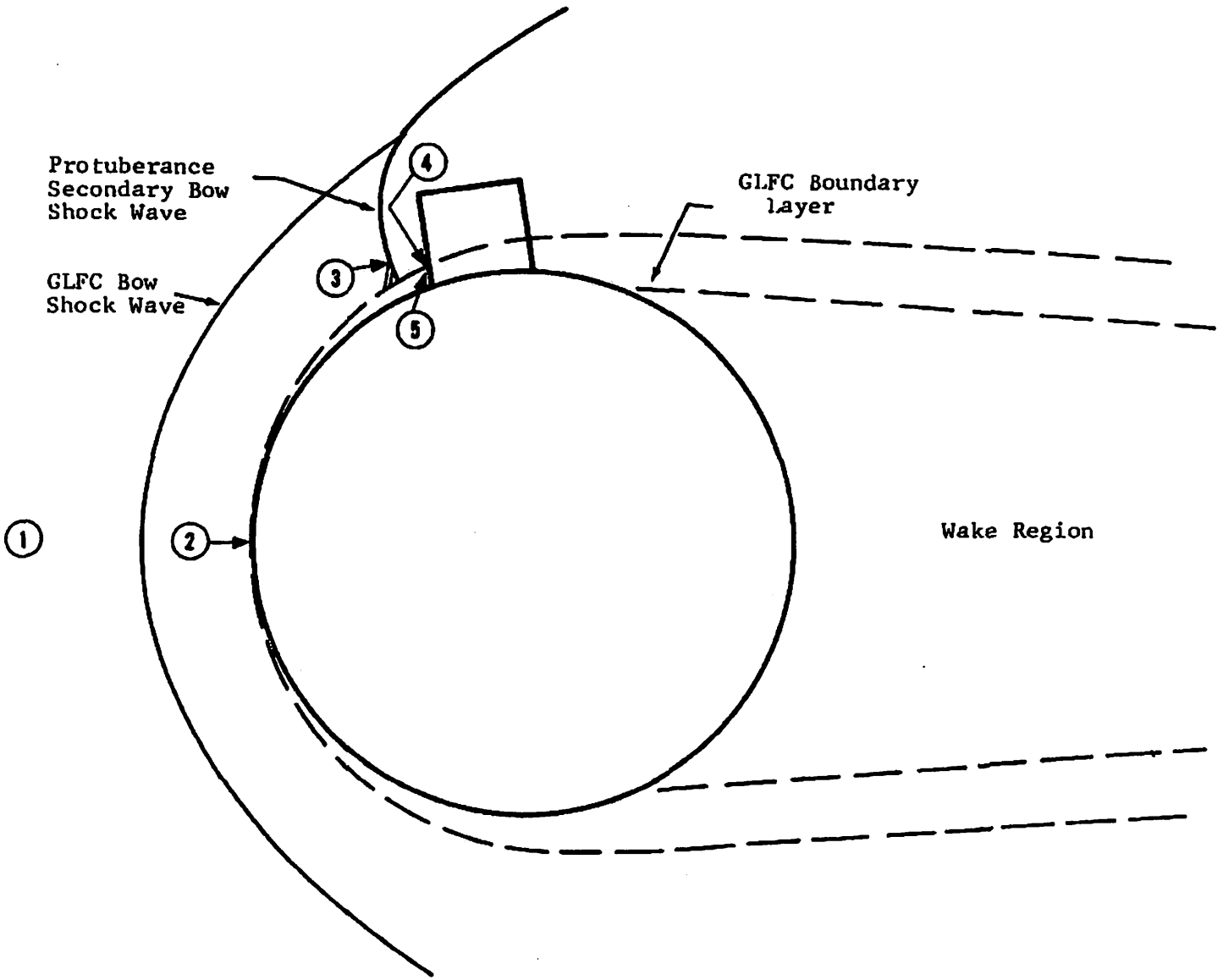

Figure 5. Flow Field Around the GLFC and Protuberance
(D68-11286)

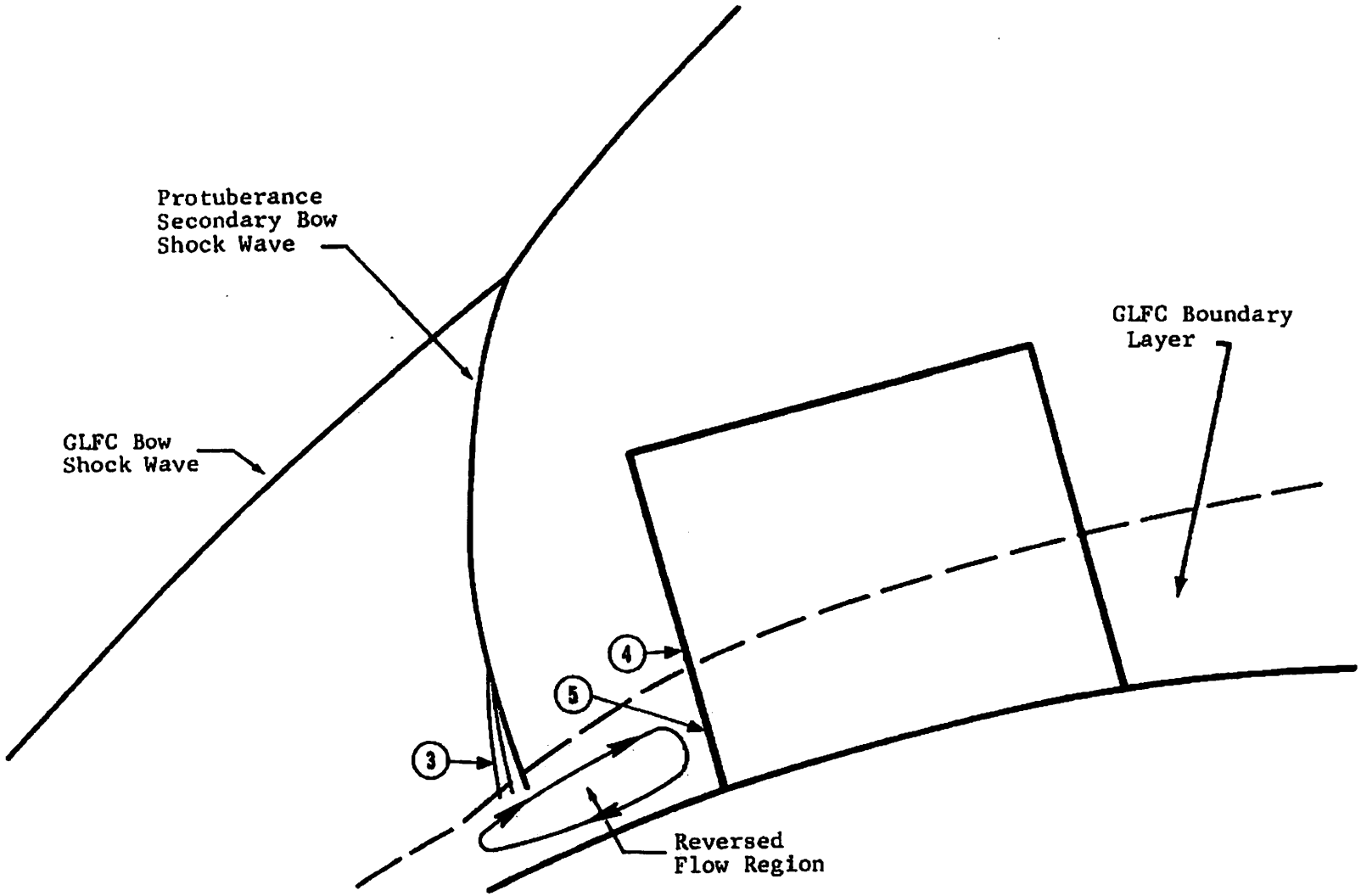

Figure 6. Flow Field Around the Protuberance
(D68-11287)

A. Orbital decay, maximum convective aerodynamic heating

P_∞ = free stream air pressure
= 0.27437 pounds per square foot

ρ_∞ = free stream air density
= 3.6531×10^{-7} slugs per cubic foot

T_∞ = free stream air temperature
= 437.707 °R

V_∞ = free stream air velocity
= 20,000 feet per second

B. Orbital decay, maximum deceleration

P_∞ = 2.8421 pounds per square foot

ρ_∞ = 3.4574×10^{-6} slugs per cubic foot

T_∞ = 479.073 °R

V_∞ = 10,000 feet per second

C. Shallow supercircular reentry, maximum convective aerodynamic heating

P_∞ = 0.41348 pounds per square foot

ρ_∞ = 5.2730×10^{-7} slugs per cubic foot

T_∞ = 456.999 °R

V_∞ = 31,000 feet per second

D. Shallow supercircular reentry, maximum deceleration

P_∞ = 1.3298 pounds per square foot

ρ_∞ = 1.5908×10^{-6} slugs per cubic foot

T_∞ = 487.170 °R

V_∞ = 23,000 feet per second

E. Steep supercircular reentry, maximum convective aerodynamic heating

P_∞ = 4.2066 pounds per square foot

ρ_∞ = 5.2844×10^{-6} slugs per cubic foot

T_∞ = 463.923 °R

V_∞ = 31,000 feet per second

F. Steep supercircular reentry, maximum deceleration

P_∞ = 20.314 pounds per square foot

ρ_∞ = 2.8862×10^{-5} slugs per cubic foot

T_∞ = 410.202 °R

V_∞ = 20,000 feet per second

The conditions presented above are at location (1) in Figure 5.

Stagnation Conditions Behind the GLFC Bow Shock Wave

Once the free stream conditions ahead of the GLFC bow shock wave are defined, the stagnation conditions behind the GLFC bow shock wave must be computed. Ideally, a real-gas nonequilibrium flow field program would be used to compute these conditions. Unfortunately, the limited time available for the analysis did not allow this. Therefore, real-gas equilibrium continuum flow normal shock tables (Reference 8) for the 1962 U.S. Standard Atmosphere were used to define the stagnation conditions behind the GLFC shock wave. While the GLFC bow shock wave is curved, one is interested in the gas properties in the GLFC boundary layer. The streamlines which enter the boundary layer cross the bow shock near the stagnation streamline where the bow shock is almost normal. Thus, use of the normal shock tables is justified.

The values of (POP/P1), (ROP/R1), (TOP/T1), and (GAMMEOP) were determined for each of the six trajectory conditions for the specified values of velocity and altitude. POP/P1 is the ratio of stagnation pressure behind the normal shock wave to the static pressure in front of the normal shock wave. ROP/R1 is the ratio of stagnation density behind the normal shock wave to the static density in front of the normal shock wave. TOP/T1 is the ratio of stagnation temperature behind the normal shock wave to the static temperature in front of the normal shock wave. GAMMEOP is the stagnation specific heat ratio behind the normal shock wave, γ_{T_2}, which is needed for later steps in the analysis. The stagnation pressure behind the normal shock wave, P_{T_2}, was obtained by multiplying P_∞ by (POP/P1). The stagnation density behind the normal shock wave, ρ_{T_2}, was obtained by multiplying ρ_∞ by (ROP/R1). The stagnation temperature behind the normal shock wave, T_{T_2}, was obtained by multiplying T_∞ by (TOP/T1).

The stagnation conditions behind the GLFC bow shock are presented below for the six flight conditions investigated.

A. Orbital decay, maximum convective aerodynamic heating

P_{T_2} = 127.57 pounds per square foot
ρ_{T_2} = 5.5750 x 10^{-6} slugs per cubic foot
T_{T_2} = 10,236 °R
γ_{T_2} = 1.1208

B. Orbital decay, maximum deceleration

P_{T_2} = 329.61 pounds per square foot

ρ_{T_2} = 3.2582 x 10^{-5} slugs per cubic foot

T_{T_2} = 5,527 °R

γ_{T_2} = 1.1496

C. Shallow supercircular reentry, maximum convective aerodynamic heating

P_{T_2} = 491.62 pounds per square foot

ρ_{T_2} = 8.8233 x 10^{-6} slugs per cubic foot

T_{T_2} = 16,083 °R

γ_{T_2} = 1.2232

D. Shallow supercircular reentry, maximum deceleration

P_{T_2} = 815.71 pounds per square foot

ρ_{T_2} = 2.5361 x 10^{-5} slugs per cubic foot

T_{T_2} = 11,856 °R

γ_{T_2} = 1.1357

E. Steep supercircular reentry, maximum convective aerodynamic heating

P_{T_2} = 4917.9 pounds per square foot

ρ_{T_2} = 8.3529 x 10^{-5} slugs per cubic foot

T_{T_2} = 17,249 °R

γ_{T_2} = 1.2372

F. Steep supercircular reentry, maximum deceleration

P_{T_2} = 11,149 pounds per square foot

ρ_{T_2} = 3.7124 x 10^{-4} slugs per cubic foot

T_{T_2} = 12,643 °R

γ_{T_2} = 1.1515

The conditions presented above are at location (2) in Figure 5.

Local Free Stream Conditions in Front of the Protuberance Secondary Bow Shock Wave

If a real-gas nonequilibrium flow field code had been used in the preceding section, the local conditions at a point 73.5 degrees away from the stagnation line would now be known. Unfortunately, time did not permit doing this, and the local free stream conditions in front of the protuberance secondary bow shock wave must now be calculated.

The local conditions at 73.5 degrees away from the stagnation line were calculated using an isentropic expansion at constant ratio of specific heats, γ, at a value of γ equal to the stagnation point γ. To use this approach, the local pressure at the point of interest must be calculated.

Newtonian theory (Reference 9) was used to calculate the ratio of local pressure, P_L, to stagnation pressure behind the GLFC bow shock wave, P_{T_2}. This ratio, P_L/P_{T_2}, was 0.0806.

The Sandia Quicktran remote terminal facility, with the IBM 7040/44 computer in Los Angeles, was used to calculate the local flow properties at location (3). Computer code HRS009 was written, and the first part of this code contained the necessary equations to calculate the isentropic expansion of a gas at constant ratio of specific heats.

The pertinent equations (Reference 10) are:

$$M_L = \left\{ \frac{2}{\gamma_{T_2} - 1} \left[\left(\frac{P_{T_2}}{P_L} \right)^{\frac{\gamma_{T_2} - 1}{\gamma_{T_2}}} - 1 \right] \right\}^{1/2} \tag{1}$$

where:

M_L = local Mach number at a location just in front of the secondary bow shock wave in front of the protuberance, outside the boundary layer.

$$\frac{T_L}{T_{T_2}} = \left(\frac{P_L}{P_{T_2}} \right)^{\frac{\gamma_{T_2} - 1}{\gamma_{T_2}}} \tag{2}$$

where:

T_L = local static temperature at a location just in front of the secondary bow shock wave in front of the protuberance, outside the boundary layer.

$$\frac{\rho_L}{\rho_{T_2}} = \left(\frac{P_L}{P_{T_2}}\right)^{\frac{1}{\gamma_{T_2}}} \tag{3}$$

where:

ρ_L = local static density at a location just in front of the secondary bow shock wave in front of the protuberance, outside the boundary layer.

$$\alpha_L = 49.02 \left(\frac{\gamma_{T_2}}{1.4} T_L\right)^{1/2} \tag{4}$$

where:

α_L = local speed of sound at a location just in front of the secondary bow shock wave in front of the protuberance, outside the boundary layer.

$$U_L = M_L \alpha_L \tag{5}$$

where

U_L = local air speed at a location just in front of the secondary bow shock wave in front of the protuberance, outside the boundary layer.

These five equations, with the stagnation flow conditions behind the GLFC bow shock wave, allowed computer calculation of the local flow properties at a location just in front of the protuberance bow shock wave outside the boundary layer. The results for the six flight conditions investigated are presented below.

A. Orbital decay, maximum convective aerodynamic heating

P_L = 10.285 pounds per square foot
ρ_L = 0.58946 x 10^{-6} slugs per cubic foot
T_L = 7,803 °R
M_L = 2.2721
U_L = 8,803 feet per second

B. Orbital decay, maximum deceleration

P_L = 26.566 pounds per square foot

ρ_L = 0.36442 x 10^{-5} slugs per cubic foot

T_L = 3982 °R

M_L = 2.2769

U_L = 6,382 feet per second

C. Shallow supercircular reentry, maximum convective aerodynamic heating

P_L = 39.623 pounds per square foot

ρ_L = 0.11259 x 10^{-5} slugs per cubic foot

T_L = 10,158 °R

M_L = 2.2862

U_L = 10,558 feet per second

D. Shallow supercircular reentry, maximum deceleration

P_L = 65.745 pounds per square foot

ρ_L = 0.27616 x 10^{-5} slugs per cubic foot

T_L = 8,775 °R

M_L = 2.2747

U_L = 9,408 feet per second

E. Steep supercircular reentry, maximum convective aerodynamic heating

P_L = 396.38 pounds per square foot

ρ_L = 0.10910 x 10^{-4} slugs per cubic foot

T_L = 10,644 °R

M_L = 2.2875

U_L = 10,875 feet per second

F. Steep supercircular reentry, maximum deceleration

P_L = 898.58 pounds per square foot

ρ_L = 0.41671 x 10^{-4} slugs per cubic foot

T_L = 9,078 °R

M_L = 2.2772

U_L = 9,645 feet per second

The conditions presented above are at location (3) in Figures 5 and 6.

Stagnation Conditions Behind the Protuberance
Secondary Bow Shock Wave

To compute the stagnation conditions behind the protuberance secondary bow shock wave, the Sandia Quicktran facility was used. The following equations were transmitted to the computer as the second part of computer code HRS009.

$$P_{T_2}' = P_{T_2} \left[\frac{\left(\gamma_{T_2} + 1\right) M_L^2}{\left(\gamma_{T_2} - 1\right) M_L^2 + 2} \right]^{\frac{\gamma_{T_2}}{\gamma_{T_2} - 1}} \left[\frac{\gamma_{T_2} + 1}{2\gamma_{T_2} M_L^2 - \left(\gamma_{T_2} - 1\right)} \right]^{\frac{1}{\gamma_{T_2} - 1}} \tag{6}$$

where:

P_{T_2}' = local stagnation pressure behind the normal part of the secondary bow shock wave in front of the protuberance but outside the boundary layer.

$$T_{T_2}' = T_{T_2} \tag{7}$$

where:

T_{T_2}' = local stagnation pressure behind the normal part of the secondary bow shock wave in front of the protuberance but outside the boundary layer.

$$\rho_{T_2}' = \rho_{T_2} \frac{P_{T_2}'}{P_{T_2}} \tag{8}$$

where:

ρ_{T_2}' = local stagnation density behind the normal part of the secondary bow shock wave in front of the protuberance but outside the boundary layer.

Equations 6 and 7 (Reference 10) are for a gas which is calorically perfect, which is the assumption of constant specific heats. Equation 8 corresponds to the assumption of a gas which is thermally perfect.

These three equations, with the local flow conditions at a location just in front of the protuberance and its bow shock wave but outside the boundary layer, allow computer calculation of stagnation properties at a location behind the normal part of the secondary bow shock wave in front of the protuberance but outside the boundary layer. The results for the six flight conditions investigated are as follows.

A. Orbital decay, maximum convective aerodynamic heating

$P_{T_2}'/P_{T_2} = 0.49441$

$P_{T_2}' = 63.086$ pounds per square foot

$\rho_{T_2}' = 0.27563 \times 10^{-5}$ slugs per cubic foot

$T_{T_2}' = 10{,}236$ °R

B. Orbital decay, maximum deceleration

$P_{T_2}'/P_{T_2} = 0.50479$

$P_{T_2}' = 166.38$ pounds per square foot

$\rho_{T_2}' = 0.16446 \times 10^{-4}$ slugs per cubic foot

$T_{T_2}' = 5{,}527$ °R

C. Shallow supercircular reentry, maximum convective aerodynamic heating

$P_{T_2}'/P_{T_2} = 0.53026$

$P_{T_2}' = 260.68$ pounds per square foot

$\rho_{T_2}' = 0.46785 \times 10^{-5}$ slugs per cubic foot

$T_{T_2}' = 16{,}083$ °R

D. Shallow supercircular reentry, maximum deceleration

$P_{T_2}'/P_{T_2} = 0.49981$

$P_{T_2}' = 407.69$ pounds per square foot

$\rho_{T_2}' = 0.12675 \times 10^{-4}$ slugs per cubic foot

$T_{T_2}' = 11{,}856°R$

E. Steep supercircular reentry, maximum convective aerodynamic heating

$P_{T_2}'/P_{T_2} = 0.53493$

$P_{T_2}' = 2{,}630.8$ pounds per square foot

$\rho_{T_2}' = 0.44678 \times 10^{-4}$ slugs per cubic foot

$T_{T_2}' = 17{,}249$ °R

F. Steep supercircular reentry, maximum deceleration

$P_{T_2}'/P_{T_2} = 0.50546$

$P_{T_2}' = 5{,}635.2$ pounds per square foot

$\rho_{T_2}' = 0.18763 \times 10^{-3}$ slugs per cubic foot

$T_{T_2}' = 12{,}643$ °R

The conditions presented above are at location 4 in Figures 5 and 6.

Reference Conditions in the Reversed Flow Region

In the reference enthalpy approach to the solution of boundary layer equations, the constant property boundary layer solution is used with the properties evaluated at a reference enthalpy. In regions where the local free stream velocity is small, the reference enthalpy can be approximated by (Reference 11):

$$h^* = \frac{1}{2}\left(h_e + h_w\right) \tag{9}$$

where:

h^* = reference enthalpy

h_e = enthalpy at the outer edge of the boundary layer

h_w = enthalpy at the wall temperature

One is interested in the heating rates to the titanium bands when they are near the melt temperature of titanium, so a wall temperature of 3,000°R was used for all calculations. Assuming that, for the low local velocities and the high static temperatures in the region of interest, the enthalpy is proportional to temperature and that the local total enthalpy at the outer edge of the boundary layer is approximately equal to the free stream total enthalpy ahead of the GLFC bow shock, the reference enthalpy and reference temperature, T*, can be evaluated. Computer code HRS011A was used with the Sandia Quicktran facility to compute the local enthalpy at the edge of the boundary layer.

The pressure is essentially constant across the boundary layer; this results in:

$$P^* = P_{T_2}' \tag{10}$$

where:

P* = reference pressure or "average" boundary layer pressure.

Using the equation of state for a gas which is thermally perfect results in:

$$\rho^* = \rho_{T_{T_2}'} \frac{T_{T_2}'}{T^*} \tag{11}$$

where:

ρ* = reference density or "average" boundary layer density.

As is apparent in the following section of this report, the reference viscosity, μ*, is needed in order to calculate the local heating in front of the protuberance. To evaluate μ*, an empirical approximation (Reference 12) of the viscosity of equilibrium air was used. This approximation presents μ as a function of P and h. Computer code HRS011B, based on Reference 12, was written and used with the Sandia Quicktran facility to evaluate μ*.

The reference properties or "average" properties in the boundary layer immediately in front of the protuberance for the six flight conditions investigated are as follows.

A. Orbital decay, maximum convective aerodynamic heating
   $P^* = 63.086$ pounds per square foot
   $\rho^* = 0.43527 \times 10^{-5}$ slugs per cubic foot
   $T^* = 6{,}618$ °R
   $h^* = 5{,}159$ BTU per pound
   $\mu^* = 0.84248 \times 10^{-4}$ pound mass per foot second

B. Orbital decay, maximum deceleration
   $P^* = 166.38$ pounds per square foot
   $\rho^* = 0.213 \times 10^{-4}$ slugs per cubic foot
   $T^* = 4{,}263$ °R
   $h^* = 1{,}109$ BTU per pound
   $\mu^* = 0.47854 \times 10^{-4}$ pound mass per foot second

C. Shallow supercircular reentry, maximum convective aerodynamic heating
   $P^* = 260.68$ pounds per square foot
   $\rho^* = 0.78800 \times 10^{-5}$ slugs per cubic foot
   $T^* = 9{,}541$ °R
   $h^* = 11{,}875$ BTU per pound
   $\mu^* = 0.12035 \times 10^{-3}$ pound mass per foot second

D. Shallow supercircular reentry, maximum deceleration
   $P^* = 407.69$ pounds per square foot
   $\rho^* = 0.202 \times 10^{-4}$ slugs per cubic foot
   $T^* = 7{,}428$ °R
   $h^* = 6{,}611$ BTU per pound
   $\mu^* = 0.97029 \times 10^{-4}$ pound mass per foot second

E. Steep supercircular reentry, maximum convective aerodynamic heating
   $P^* = 2{,}630.8$ pounds per square foot
   $\rho^* = 0.760 \times 10^{-4}$ slugs per cubic foot
   $T^* = 10{,}124$ °R
   $h^* = 11{,}250$ BTU per pound
   $\mu^* = 0.12818 \times 10^{-3}$ pound mass per foot second

F. Steep supercircular reentry, maximum deceleration

$P^* = 5{,}635.2$ pounds per square foot

$\rho^* = 0.304 \times 10^{-3}$ slugs per cubic foot

$T^* = 7{,}821$ °R

$h^* = 4{,}935$ BTU per pound

$\mu^* = 0.92190 \times 10^{-4}$ pound mass per foot second

The conditions presented above are at location (5) in Figures 5 and 6.

Calculation of the Aerodynamic Heating Rate Distribution in Front of the Protuberance

In any aerodynamic analysis, the first step is to conduct a literature search to see what experimental and theoretical work already exists. A brief literature search yielded References 13 through 22.

References 13 through 16 present experimental data on convective aerodynamic heating to protuberances on several shapes. (For the velocities and small protuberance size in this analysis, radiative aerodynamic heating can be neglected.) Reference 17, with supplemental information in References 18 through 22, presents an empirically modified theoretical boundary layer approximation of the reversed flow region convective aerodynamic heating. This empirically modified theoretical approximation shows good agreement with measured data from several sources. In particular, good agreement is shown with the comprehensive experimental results presented in Reference 13. Therefore, this empirically modified theoretical method was used for the calculations.

The local skin friction coefficient is:

$$C_{F_\ell} = 0.664\,\alpha \left(\frac{\rho^* \ \mu^*}{\rho_L \ \mu_L}\right)^{0.5} \left(\frac{\mu_L}{U_L \ \rho_L \ X}\right)^{0.5} \tag{12}$$

where:

C_{F_ℓ} = local skin friction coefficient

α = empirical factor to account for adverse pressure gradient

X = distance forward from protuberance

From Reynolds analogy, assuming a Prandtl number of 1, one gets:

$$C_{H_\ell} = \frac{C_{F_\ell}}{2} \tag{13}$$

where:

C_{H_ℓ} = local heat transfer coefficient.

Also,

$$\dot{q}_{w_\ell} = C_{H_\ell} \rho_\ell U_\ell \left(h_\ell - h_w\right) \tag{14}$$

where:

$\dot{q}_{w_\ell}$ = local heat transfer rate to wall

h_ℓ = local recovery enthalpy

For the assumption of a Prandtl number of 1, the local recovery enthalpy can be replaced by the free stream total enthalpy.

Equation 14, for a given flight condition, can be expressed by:

$$\dot{q}_{w_\ell} = \frac{C_1}{\sqrt{X}} \quad . \tag{15}$$

Thus, with the assumptions made above, and with a value of α of 3.8 (Reference 17), Equations 12 through 15 define the local heat transfer distribution in front of the protuberance.

Computer code HRS013 was written and was used with the Sandia Quicktran facility to calculate the local heat transfer rates in front of the protuberance for the six flight conditions. (The flow field properties were assumed constant in the reversed flow region.) The results are summarized below, where the values of C_1 are presented for each of the six flight conditions.

A. Orbital decay, maximum convective aerodynamic heating
   C_1 = 102.250 BTU per foot $^{1.5}$ second

B. Orbital decay, maximum deceleration
C_1 = 36.440 BTU per foot $^{1.5}$ second

C. Shallow supercircular reentry, maximum convective aerodynamic heating
C_1 = 434.372 BTU per foot $^{1.5}$ second

D. Shallow supercircular reentry, maximum deceleration
C_1 = 324.386 BTU per foot $^{1.5}$ second

E. Steep supercircular reentry, maximum convective aerodynamic heating
C_1 = 1,412.659 BTU per foot $^{1.5}$ second

F. Steep supercircular reentry, maximum deceleration
C_1 = 939.201 BTU per foot $^{1.5}$ second

Figure 7 presents the heat transfer distribution in front of the protuberance for the orbital decay reentry at maximum convective aerodynamic heating. Distributions are not presented for the other flight conditions because they differ from Figure 7 only by a constant.

Calculation of the "Average" Aerodynamic Heating Rate in Front of the Protuberance

The convective aerodynamic heating rate in front of the protuberance was calculated in the preceding section. However, the Sandia Charring Material Ablator (CMA) Program, which would be used for the ablation analysis of the GLFC graphite shell, is currently only one-dimensional, and a heating rate distribution to the GLFC ahead of the protuberance cannot be used as input data.

To obtain an "average" value of the heat transfer rate in front of the protuberance, Equation 12 can be integrated with respect to X and divided by X. (As in the preceding section, the flow field properties are assumed to be constant in the reversed flow region.) After Equation 12 is integrated, the results are:

$$C_{F_{\ell_a}} = 1.328\,\sigma \left(\frac{\rho^* \mu^*}{\rho_L \mu_L}\right)\left(\frac{\mu_L}{U_L \rho_L X}\right) \tag{16}$$

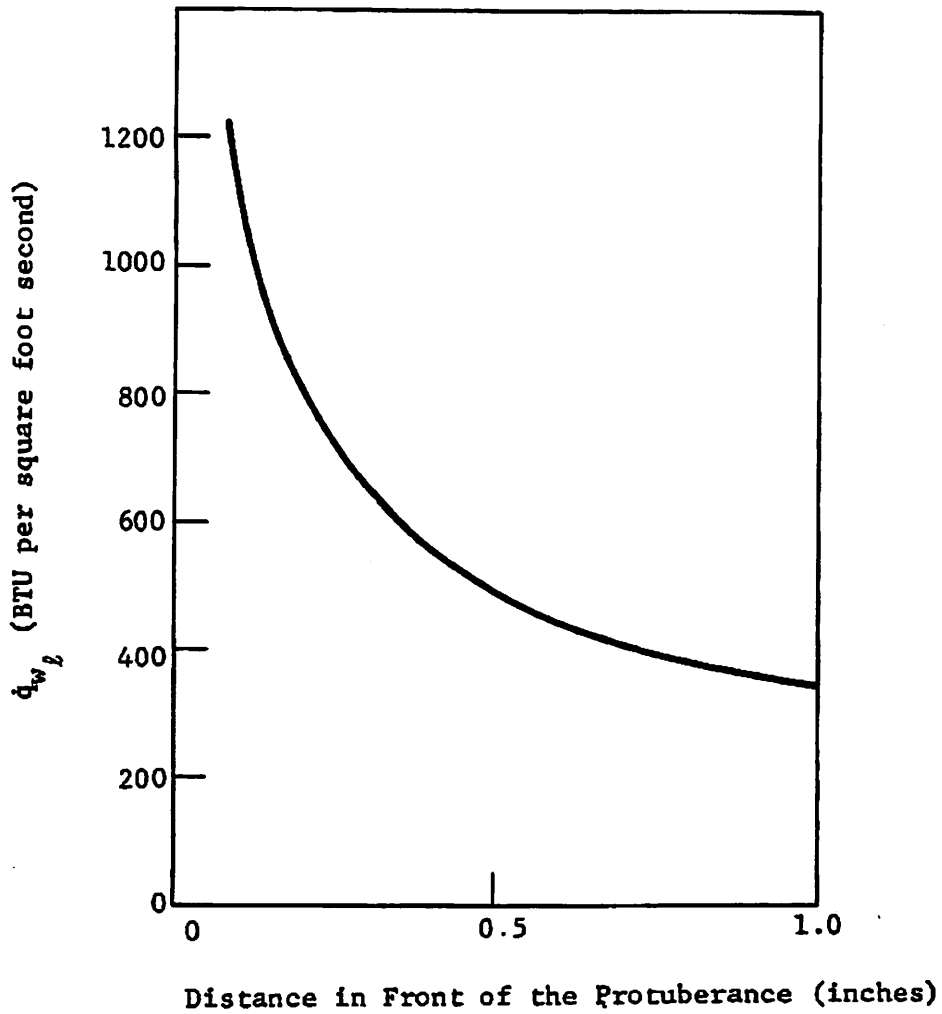

Figure 7. Local Wall Heat Transfer Rate as a Function of Distance in Front of the Protuberance, Orbital Decay, Maximum Convective Aerodynamic Heating (D68-11288)

where:

$C_{F_{\ell_{average}}}$ = local "average" skin friction coefficient from 0 to X,

or:

$$C_{F_{\ell_{average}}} = 2\ C_{F_\ell} \quad . \tag{17}$$

From Reynolds analogy and assuming a Prandtl number of 1:

$$C_{H_{\ell_{average}}} = \frac{C_{F_{\ell_{average}}}}{2} \tag{18}$$

where:

$C_{H_{\ell_{average}}}$ = local "average" heat transfer coefficient from 0 to X,

and

$$\dot{q}_{w_{\ell_{average}}} = C_{H_{\ell_{average}}}\ \rho_\ell\left(h_\ell - h_w\right) \tag{19}$$

where:

$\dot{q}_{w_{\ell_{average}}}$ = local "average" heat transfer rate to the wall from 0 to X.

Thus,

$$\dot{q}_{w_{\ell_{average}}} = 2\dot{q}_{w_\ell} = \frac{2C_1}{\sqrt{X}} \quad . \tag{20}$$

Figure 8 presents the average heat transfer rate, as a function of X, in front of the protuberance for the orbital decay reentry at maximum convective aerodynamic heating. Average heat transfer rates are not presented for the other flight conditions because they would differ from Figure 8 only by a constant.

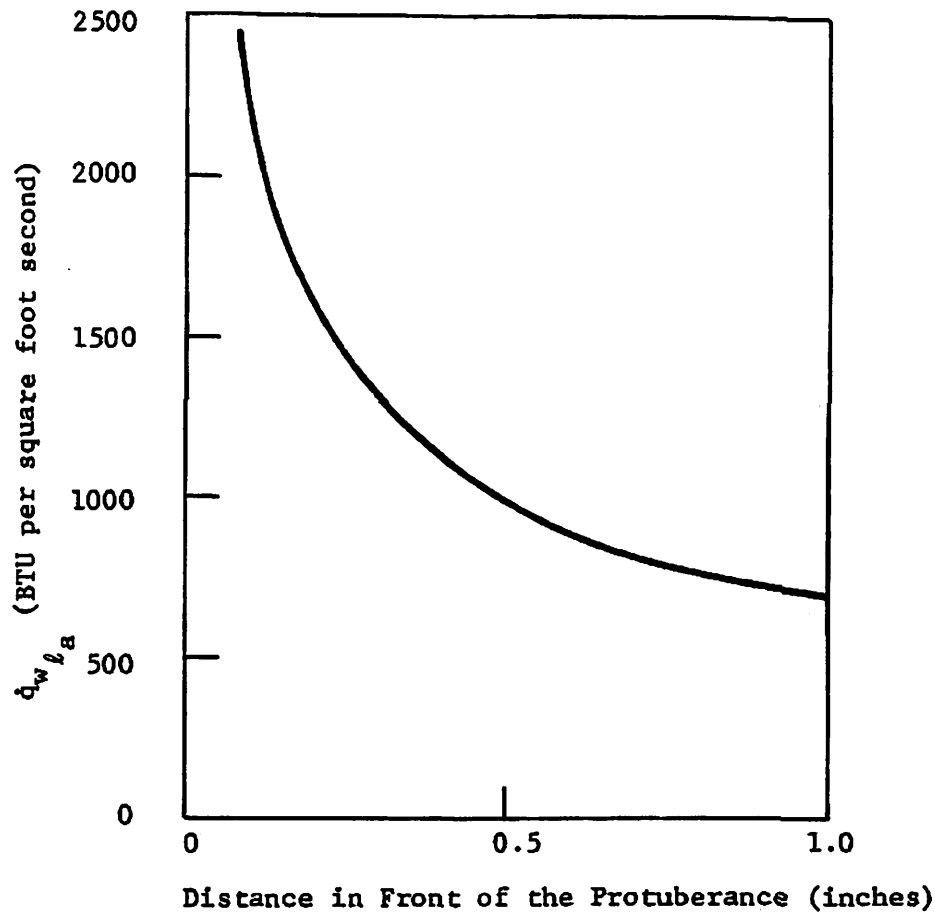

Figure 8. Local "Average" Wall Heat Transfer Rate as a Function of Distance in Front of the Protuberance, Orbital Decay, Maximum Convective Aerodynamic Heating (D68-11289)

Now, a value of X must be selected to define the "average" heat transfer rate to the GLFC in front of the protuberance. Since the graphite cask thickness is 0.350 inch in the region of interest, an X of one-third inch was selected to permit the one-dimensional ablation and conduction heat transfer solution to be a realistic approximation of the actual three-dimensional problem.

For this value of X, Equation 20 can be rewritten as:

$$\dot{q}_{w_{average}} = 12C_1 \tag{21}$$

where:

$\dot{q}_{w_{average}}$ = "average" heat transfer rate to the wall from X = 0 to X = 0.33 inch.

The resultant values of $\dot{q}_{w_{average}}$ for the six flight conditions are presented below.

A. Orbital decay, maximum convective aerodynamic heating
$\dot{q}_{w_{average}}$ = 1227.00 BTU per square foot second

B. Orbital decay, maximum deceleration
$\dot{q}_{w_{average}}$ = 437.28 BTU per square foot second

C. Shallow supercircular reentry, maximum convective aerodynamic heating
$\dot{q}_{w_{average}}$ = 5212.46 BTU per square foot second

D. Shallow supercircular reentry, maximum deceleration
$\dot{q}_{w_{average}}$ = 3892.63 BTU per square foot second

E. Steep supercircular reentry, maximum convective aerodynamic heating
$\dot{q}_{w_{average}}$ = 16,951.91 BTU per square foot second

F. Steep supercircular reentry, maximum deceleration
$\dot{q}_{w_{average}}$ = 11,246.41 BTU per square foot second

Calculation of the Ratio of "Average" Aerodynamic Heating in Front of the Protuberance to the Stagnation Line Aerodynamic Heating Rate to the GLFC

The stagnation line aerodynamic convective heating rate to the GLFC was previously calculated as a function of time for the trajectories of interest. It is desirable to compute the ratio of the "average" aerodynamic convective heating rate in front of the protuberance to the stagnation line aerodynamic convective heating rate of the GLFC for the six flight conditions. If this ratio is reasonably constant during a trajectory, it can be used to convert the previously computed stagnation line convective aerodynamic heating rate to the "average" convective aerodynamic heating rate in front of the protuberance.

The equation for the stagnation point aerodynamic convective heating rate to the stagnation point of a sphere, for ionized equilibrium flow downstream of the bow shock wave, is (Reference 23):

$$\dot{q}_{s_s} = \frac{17,600}{\sqrt{R_N}} \left(\frac{\rho_\infty}{\rho_o}\right)^{1/2} \left(\frac{V_\infty}{25,954}\right)^{3.15} \tag{22}$$

where:

$\dot{q}_{s_s}$ = cold wall stagnation point aerodynamic heating rate to a sphere of radius R_N, BTU per square foot second

R_N = sphere radius, feet

ρ_o = sea level standard atmospheric density, 0.002378 slugs per cubic foot.

The above equation, as computer code HRS010, was used with the Sandia Quicktran facility to compute $\dot{q}_{s_s}\sqrt{R_N}$ for the six flight conditions. $\dot{q}_{s_s}$ can be obtained by dividing by the square root of the cylinder radius, 0.3333 feet.

Based on the assumption of a Newtonian theory velocity gradient near the stagnation point, it can be shown that (Reference 24):

$$\dot{q}_{s_c} = \frac{1}{\sqrt{2}} \dot{q}_{s_s} \tag{23}$$

where:

$\dot{q}_{s_c}$ = cold wall stagnation point aerodynamic heating rate to a cylinder of radius R_N, BTU per square foot second.

Thus, $\dot{q}_{s_c}$ can be computed.

Once having determined $\dot{q}_{w_{\ell a}}$ and $\dot{q}_{s_c}$, the ratio of $\dot{q}_{w_{\ell a}}$ to $\dot{q}_{s_c}$ can be computed. The values of $\dot{q}_{s_c}$ and $\dot{q}_{w_{\ell a}}/\dot{q}_{s_c}$ are presented below for each of the six flight conditions.

A. Orbital decay, maximum convective aerodynamic heating

$\dot{q}_{s_c}$ = 118 BTU per square foot second

$\dot{q}_{w_{\ell a}}/\dot{q}_{s_c}$ = 10.4

B. Orbital decay, maximum deceleration

$\dot{q}_{s_c}$ = 41 BTU per square foot second

$\dot{q}_{w_{\ell a}}/\dot{q}_{s_c}$ = 10.6

C. Shallow supercircular reentry, maximum convective aerodynamic heating

$\dot{q}_{s_c}$ = 565 BTU per square foot second

$\dot{q}_{w_{\ell a}}/\dot{q}_{s_c}$ = 9.2

D. Shallow supercircular reentry, maximum deceleration

$\dot{q}_{s_c}$ = 383 BTU per square foot second

$\dot{q}_{w_{\ell a}}/\dot{q}_{s_c}$ = 10.2

E. Steep supercircular reentry, maximum convective aerodynamic heating

$\dot{q}_{s_c}$ = 1785 BTU per square foot second

$\dot{q}_{w_{\ell a}}/\dot{q}_{s_c}$ = 9.5

F. Steep supercircular reentry, maximum deceleration

$\dot{q}_{s_c}$ = 1050 BTU per square foot second

$\dot{q}_{w_{\ell_a}} / \dot{q}_{s_c} = 10.7$

The information presented above provides the information needed as input data for the ablation analysis of the GLFC.

Conclusions

As shown in the previous section, the "average" local convective aerodynamic heating rate in front of the protuberance is approximately 10 times the stagnation line convective aerodynamic heating rate to the GLFC in crossflow. This ratio varied from 9.2 to 10.7 for the six flight conditions examined. One would expect these values to be relatively independent of flight conditions on the basis of the hypersonic Mach number independence principle.

While these values appear high, being approximately 33 times the local rate to the GLFC without protuberance, these values are reasonable. Previous Sandia tests to define the effects of protuberances on heating rates (Reference 16) showed that local rates without protuberances can be increased over 20 times with the addition of protuberances. These same tests showed the "average" local heating rate in front of the protuberance to be approximately 5 times the stagnation heating rate to this configuration.

Any additional theoretical work in this area, on a longer time scale, should:

1. Look at the effect of the pressure gradient around the cylinder on α in Equation 12.
2. Attempt to replace the assumption of constant properties in the separated flow region with a more realistic variation.
3. Attempt to place a realistic limit on the maximum heating rate in front of the protuberance (i.e., replace the infinite singularity at X = 0 with a finite value).
4. If possible, utilize a real gas nonequilibrium flow field computer program to calculate the flow field around the GLFC and, if possible, ahead of the protuberance.

5. Utilize any two-dimensional and three-dimensional heat transfer and ablation options developed for the CMA computer code.

6. Extend the analysis to both higher altitudes and the transition flow regime.

7. Include the effects of finite shock detachment distances ahead of the protuberance on the calculation of conditions at locations (3), (4), and (5).

Obviously, experimental test results would provide much needed information regarding the increased heating from the protuberance.

REFERENCES

1. "NASA Given Lunar Surface Experiment Demonstration," William J. Normyle, Aviation Week and Space Technology, July 25, 1966.

2. "ALSEP Array Cut For First Moon Missions," Roderick D. Hibben, Aviation Week and Space Technology, April 3, 1967.

3. SC-RR-67-150, Aerodynamic And Trajectory Analyses Of A SNAP-27 Graphite Fuel Cask, H. R. Spahr, Sandia Corporation, May 1967.

4. SC-RR-67-123, A Closed Form Approximate Solution For The Initial Reentry Angle And Velocity Of Objects Decaying From Circular Orbits Around An Oblate Rotating Planet (Evaluated For Earth For Six Atmospheric Models), H. R. Spahr, Sandia Corporation, Albuquerque, New Mexico, October 1967.

5. SC-RR-67-858, Computer Code HRS004 - A Code For The Computation Of The Initial Reentry Angle And Velocity Of Objects Decaying From Earth Orbit, H. R. Spahr, Sandia Corporation, Albuquerque, New Mexico, December 1967.

6. Drawing Number BSX-5595, Layout, Cask Assembly, The Bendix Corporation, Systems Division, Ann Arbor, Michigan.

7. U.S. Standard Atmosphere, 1962, U.S. Government Printing Office, Washington, D. C., December 1962.

8. AEDC-TDR-64-214, Altitude - Velocity Tables And Charts For Imperfect Air, Clark H. Lewis and E. G. Burgess III, Arnold Engineering Development Center, Arnold Air Force Station, Tennessee, January 1965.

9. Hypersonic Flow Theory, Volume 1, Inviscid Flows, Wallace D. Hayes and Ronald F. Probstern, Academic Press, New York, Second Edition, 1966.

10. Report 1135, Equations, Tables, And Charts For Compressible Flow, Ames Research Staff, National Advisory Committee For Aeronautics, Ames Aeronautical Laboratory, Moffet Field, California, 1953.

11. Viscous Hypersonic Flow, Theory Of Reacting And Hypersonic Boundary Layers, William H. Dorrance, McGraw-Hill Book Company, Inc., New York, 1962.

12. "Analytical Approximations for the Density and Viscosity of Equilibrium Air," H. E. Worbs and B. D. Bolster, Journal of Spacecraft and Rockets, June 1967.

13. NASA Technical Note D-1372, Heat-Transfer And Pressure Measurements On A Flat-Plate Surface And Heat-Transfer Measurements On Attached Protuberances In A Supersonic Turbulent Boundary Layer At Mach Numbers Of 2.65, 3.51, And 4.44, Paige B. Burbank, Robert A. Newlander, And Ida K. Collins, Langley Research Center, National Aeronautics And Space Administration, Washington, D.C., December 1962.

14. NASA Technical Note D-2028, Heat-Transfer And Pressure Investigation Of A Fin-Plate Interference Model At A Mach Number of 6, Robert A. Jones, Langley Research Center, National Aeronautics And Space Administration, Washington, D.C., July 1964.

15. NASA Technical Note D-3094, Interference Heating On A Swept Cylinder In Region Of Intersection With A Wedge At Mach Number 8, Dennis M. Bushnell, Langley Research Center, National Aeronautics And Space Administration, Washington, D.C., December 1965.

16. SC-RR-65-43, Final Report On Re-Entry Flight Demonstration Number Two, Appendix VIII-A, Department 9310, Sandia Corporation, Albuquerque, New Mexico, April 8, 1965.

17. "Heat Transfer in the Vicinity of Surface Protuberances," True E. Surber, Journal of Spacecraft and Rockets, November - December 1965.

18. "Heat Transfer in the Vicinity of Two-Dimensional Protuberances," A. Datis, B. G. Broach, and H. H. Yen, Journal of Spacecraft and Rockets, November - December 1964.

19. "On the Model of Free, Shock Separated, Turbulent Boundary Layer," A. Mager, Journal of the Institute of the Aeronautical Sciences, Volume 23, pages 181-184, 1956.

20. Report NA-60-1579, Method of Correlating Surface Heat Transfer Data In The Vicinity Of Protuberance - Flat Plate Junctions In High Speed Flows, J. S. Yoshimura, North American Aviation, Downey, California, December 1960.

REFERENCES (cont'd)

21. Report NA-61-174, Appendix A, Heat Transfer in the Vicinity of Surface Protuberances in Supersonic Flow, J. S. Yoshimura, North American Aviation, Downey, California, April 1961.

22. NASA Memorandum 10-1-58E, Turbulent Heat Transfer Coefficients in the Vicinity of Surface Protuberances, R. J. Wishlewski, Langley Research Center, National Aeronautics and Space Administration, Washington, D.C., 1958.

23. "Generalized Heat Transfer Formulas and Graphs for Nose Cone Re-Entry Into the Atmosphere," R. W. Detra and H. Hidalgo, American Rocket Society Journal, March 1961.

24. "Laminar Heat Transfer Over Blunt-Nosed Bodies at Hypersonic Flight Speeds, Lester Lees, Jet Propulsion, April 1956.

DISTRIBUTION:

TID-4500 (51st Ed.) UC-36
(196 copies)
U. S. Atomic Energy Commission
Division of Space Nuclear Systems
Space Electric Power Office
Washington, D. C. 20545
Attn: G. A. Newby, Assistant Director (1)
G. P. Dix, Chief, Safety Branch (1)
R. S. Decker, Jr., Chief, Safety Branch (1)
R. T. Carpenter, Chief, Isotope Power Systems Branch (1)
J. A. Powers, Chief, Isotope Power Systems Branch (1)
C. Johnson, Chief, Reactor Systems Branch (1)

U. S. Atomic Energy Commission
Division of Isotope Development
Washington, D. C. 20545

U. S. Atomic Energy Commission
Director of Regulation
Washington, D. C. 20545
Attn: C. K. Beck, Deputy Director (1)
F. D. Anderson, Regulation (1)

U. S. Atomic Energy Commission
Division of Biology and Medicine
Washington, D. C. 20545
Attn: J. Z. Holland, Chief, Fallout Studies Branch (1)
H. D. Bruner, Asst. Director, Medical and Health Research (1)

U. S. Atomic Energy Commission
Space Nuclear Propulsion Office
Albuquerque Extension
Albuquerque Operations Office
P.O. Box 5400
Albuquerque, New Mexico 87115
Attn: H. P. Smith

U. S. Atomic Energy Commission
Albuquerque Operations Office
P.O. Box 5400
Albuquerque, New Mexico 87115
Attn: S. A. Upson, Director, Non-Nuclear Activities Division (1)
G. H. Dugger, Actg. Director, Operational Safety Division (1)

U. S. Atomic Energy Commission
Site Representative
National Aeronautics and Space Administration
Manned Space Center
Houston, Texas 77058
Attn: W. C. Remini
Bldg. 16, Code ZS-5

Donald W. Douglas Laboratories
P.O. Box 310
Richland, Washington 99352
Attn: S. P. Gydesen

Douglas Aircraft Company
Missile & Space Systems Division
3000 Ocean Park Blvd.
Santa Monica, California
Attn: Sig Gronich, Advanced Space Technology

General Electric Company
Valley Forge Space Technology Center, P.O. Box 8555
Philadelphia, Pennsylvania 19101
Attn: S. M. Scala, Room M9539 Space Sciences Lab (1)
T. F. Widmer, Advanced Nuclear Systems Operations (1)

Deputy I. G. for Insp. and Safety,
USAF, Kirtland Air Force Base,
New Mexico 87117
Attn: Col. D. C. Jameson (ASINSR)

Los Alamos Scientific Laboratory
P.O. Box 1663
Los Alamos, New Mexico 87544
Attn: Dr. L. D. P. King
Dr. Wright Langham
C. F. Metz, CMB-1
F. W. Schonfeld, CMF-5

Martin-Marietta Corporation
Martin Company
Nuclear Programs
Middle River, Maryland 21203
Attn: D. Anderson

Monsanto Research Corporation
Mound Laboratory
P.O. Box 32
Miamisburg, Ohio 45342
Attn: G. R. Grove

Thomas B. Kerr
Code RNS
National Aeronautics and Space Administration
Washington, D. C. 20545

National Aeronautics and Space Administration
Ames Research Center
Moffet Field, California
Attn: Glenn Goodwin

National Aeronautics and Space Administration
Goddard Space Flight Center
Glenn Dale Road
Greenbelt, Maryland 20771
Attn: A. W. Fihelly,
Nimbus Project

Naval Facilities Engineering Command
Department of the Navy, Code 042
Washington, D. C. 20390
Attn: Graham Hagey

Space Nuclear Propulsion Office
Lewis Research Center
21000 Brookpark Road
Cleveland, Ohio 44135
Attn: L. Nichols

TRW Systems
P.O. Box 287
Redondo Beach, California 90278
Attn: Dr. Donald Jortner

Union Carbide Corporation
Nuclear Division
P.O. Box X
Oak Ridge, Tennessee 37831
Attn: R. A. Robinson, Isotope Development Center (1)
B. R. Fish, Health Physics Division (1)

U. S. Public Health Service
Nat. CTR for Radiological Health
1901 Chapman Avenue
Rockville, Maryland 20852
Attn: Nuclear Facilities Section

J. R. Banister, 5120
J. D. Shreve, 5234
D. B. Shuster, 5600
H. E. Viney, 7130
L. E. Lamkin, 7300
A. N. Blackwell, 8146
G. A. Fowler, 9000
A. Y. Pope, 9300
Attn: V. E. Blake, 9310
H. E. Hansen, 9311
S. L. Jeffers, 9312
S. McAlees, Jr., 9314
H. R. Spahr, 9314 (3)
R. D. Klett, 9314
D. W. Larson, 9314
G. W. Stone, 9314
R. J. Everett, 9315
J. D. Appel, 9319
J. D. Appel, 9319 (ANSIC) (2)
R. C. Maydew, 9320
A. J. Clark, 9330
J. W. McKiernan, 9331
R. P. Stromberg, 9333
B. F. Hefley, 8232
B. R. Allen, 3421
L. C. Baldwin, 3412
L. L. Alpaugh, 3412
C. H. Sproul, 3428-2 (10)